Effects of thermal treatment on the mechanical and electromagnetic properties of 9Cr-1Mo steel

Kittinan Sodsai[a], Mai Noipitak[b, *], Viboon Saetang[a], Pongsak Tuengsook[a]

[a] Department of Production Engineering, Faculty of Engineering, King Mongkut's University of Technology Thonburi, Bangkok, 10140 Thailand
[b] Materials and Nondestructive Testing Laboratory (MNDT), Ratchaburi Learning Park, King Mongkut's University of Technology Thonburi, Ratchaburi, 70150 Thailand

***Corresponding Author:** mai.noi@kmutt.ac.th
https://doi.org/10.55674/jmsae.v12i1.249441

Received: 8 August 2022 | **Revised:** 24 August 2022 | **Accepted:** 17 December 2022 | **Available online:** 1 January 2023

Abstract

This paper presents the effects of thermal treatment conditions on the mechanical properties of 9Cr-1Mo steel. Each sample was normalized at 1,040 °C for 1 h prior to tempering at different temperatures for 2 hours. Three levels of tempering conditions, 600, 650, and 700 °C, were tested in this study. After treatment, the metallurgical structures of the samples were observed and characterized by optical microscope (OM), scanning electron microscope (SEM), energy dispersive X-ray spectrometer (EDS) and X-ray diffraction (XRD). Hardness and static tensile of the samples at room and elevated temperatures were also measured and analyzed. Non-destructive testing (NDT) associated with the eddy current method was employed to detect the microstructural changes of samples. The results revealed that the lath martensitic structure, lath boundaries, coarse precipitates, and prior austenite grain boundaries were found at grain boundaries and inside the matrix region. The average size of the particle and area fraction of carbide precipitates decreased with tempering temperature increases from 600 − 650 °C. The true yield stress and true ultimate tensile stress decreased while true strain increased when the tempering process was applied after the normalization. In addition, the use of the eddy current method at 100 kHz with proper conductivity could more accurately detect the microstructural changes of 9Cr-1Mo steel specimens than using the phase angle approach. The correlation coefficient of conductivity and true ultimate tensile strength was found to be 0.9459, indicating a high correlation between them.

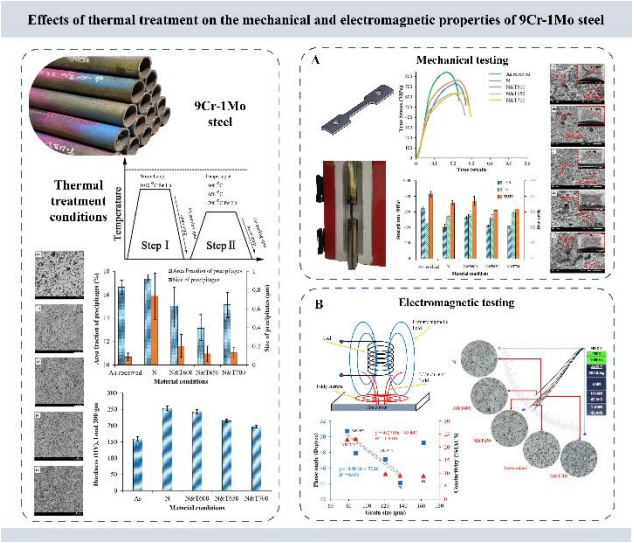

Keywords: 9Cr-1Mo steel; Electromagnetic; Static tensile testing; Elevated temperature tensile testing; Eddy current

Introduction

9Cr-1Mo steel is frequently used in the chemical and thermal power plant industry, particularly in pressure vessels used at high temperature and high pressure [1]. 9Cr-1Mo steel has remarkable creep strength, good thermal conductivity, good resistance to stress corrosion, and other beneficial mechanical properties [2 – 4]. Under an extended period of service, the operating temperature ranges from 560 − 630 °C and pressure of 220 − 300 bars [5 – 10]. This metal is usually heat-treated by the normalization and tempering (N&T) process prior to usage [11 – 12].

9Cr-1Mo steel is used in service with time as a function of operating temperature and stress. It affects various properties of the material changing due to microstructure changes which result in reduced performance during applications such as mechanical properties, rust, corrosion and other forms of heat and mass transfer in the manufacturing process [13].

For industrial, the replica technique is frequently employed to confirm the surface's microstructure of interest that can be replicated for indirect light-microscopy

inspection later. Often, field or in-situ metallography is not practical, and in some situations, it may not even be advisable to cut up the material or specimen for laboratory analysis [14 – 16]. Thus, replicas are very helpful in these situations. However, the replica technique testing procedure is highly constrained, and the tester faces chemical risks. Although this technique falls under the NDT category, the surface must be polished and ready for etching before being replicated for microscopy as part of the examination. Due to the surface preparation, especially at difficult test locations in the field, this is a relatively laborious method. Furthermore, there are obvious limitations to the surface replication technique in terms of surface, coverage, and optical resolution. In addition to the replica technique, other tests are used to evaluate materials, including the Positive Material Identification test (PMI) and portable hardness. The PMI test analyzes the chemical composition only to identify the type and grade of various types of materials, it is unable to evaluate and present the material's mechanical properties. The portable hardness test only measures the material's hardness; it is unable to evaluate and show the material's other mechanical properties.

The NDT technique with the electromagnetic method was used in the test. The eddy current method is an electromagnetic technique that has been considered a potential NDT technique for the micro-structure because the response of the magnetic field has the sensitivity to detect the microstructure of 9Cr-1Mo steel. Evaluation of microstructural changes in ferromagnetic materials, such as carbon steel, could be possible with eddy current testing. Any variation in the pearlite phase or percentage may have an impact on the material's magnetic and electric properties. The technique is conceptually based on the examination of variations in the impedance of one or more coils positioned close to the workpiece to be tested. Many researchers have studied the impact of residual stresses [17 – 22], while others have concentrated on understanding how the eddy current testing responds to microstructure changes in a variety of materials [23 – 24]. C. S. Kim [18] used the eddy current technique by measuring the reversible magnetic permeability (PMP) to evaluate of mechanical softening of the structure of ferritic 9Cr steel materials.

From previous studies, most of the engineering properties of 9Cr-1Mo steel after thermal treatment were only studied at room temperature. Additionally, there is no research that has been found to investigate the microstructural effects of 9Cr-1Mo steel after thermal treatment utilizing the phase angle and electrical conductivity technique. In the present work, the eddy current response is studied with respect to 9Cr-1Mo steel transformed during different stages of thermal treatment in each condition. The 9Cr-1Mo steel in as-received (As-received) was transformed to a different microstructure by normalizing (N) and different tempering (T) temperature conditions. Subsequently, the specimens were subjected to microstructure analysis, mechanical properties (static tensile testing at room temperature and elevated temperature tensile), and electromagnetic analysis. The results were interpreted in terms of the eddy current evaluation of microstructural changes of the steel by phase angle and electrical conductivity technique, that is indirect testing for evaluating the microstructure and mechanical properties of 9C-1Mo steel. Interpretation of the results can further be used to evaluate in-service 9Cr-1Mo steel structures.

Materials and Methods

Material and thermal treatment

This experimental study was conducted on chromium-based steel, modified 9Cr-1Mo steel (ASTM SA-213 - 9Cr-1Mo). An optical emission spectrometer (Thermo electron corporation: APL 3460) was used to analyze the 9Cr-1Mo steel chemical composition with the result detailed in Table 1 in weight percent [25 – 26]. This conforms with the ASTM A213M standard for 9Cr-1Mo steel [27].

The "as-received" 9Cr-1Mo steel tube was subjected to various thermal treatment conditions. Normalizing at 1,040 °C for 1 h, at which point a fully austenitic structure is achieved and all carbides are dissolved and then air-cooled [28 – 32]. Tempering was carried out at three different temperatures at 600, 650, and 700 °C for 2 h at a heating rate of 10 °C min^{-1} and then air-cooled to ambient temperature. Table 2 presents the normalizing and tempering heat treatment process for the specimen exposure of the test material.

Table 1 Chemical composition of 9Cr-1Mo steel tube in as-received (wt%).

Fe	C	Mn	P	S	Si	Cr	Mo	V	Cb/Nb	Ni	Al
88.86	0.112	0.447	0.011	0.004	0.294	8.667	0.861	0.232	0.083	0.131	0.012

Structural analysis setup

This research integrated the physical and mechanical properties of 9Cr-1Mo steel with thermal treatment and thermal testing using OM, SEM, hardness, tensile and electromagnetic with the commercial eddy current (CEC) technique. The microstructure characterization of the 9Cr-1Mo steel specimen was analyzed using the OM and SEM (JEOL: JSM-6610 LV) with energy-dispersive X-ray spectroscopy (EDS) (OXFORD: INCAx-act). The 9Cr-1Mo steel was polished using emery paper up to a grit size number 1,200, then removing the emery paper scratches using alumina powder-coated cloth polishing. After polishing, all samples were etched by 3% Nital. The fraction area of carbide precipitates and particle size of carbide was measured using the Image-J software. For phase determination of 9Cr-1Mo steel in various normalizing and tempering conditions, a D-2 phaser Bruker X-ray diffractometer was employed to conduct X-ray diffraction (XRD) analysis by using the Cu-target, and the working voltage and current were 30 kV and 10 mA, respectively.

Table 2 The thermal treatment of 9Cr-1Mo steel in each material condition**.**

Material condition	Normalization temperature	Tempering temperature
As-received	-	-
N	1,040°C for 1 h	-
N&T600	1,040°C for 1 h	600°C for 2 h
N&T650	1,040°C for 1 h	650°C for 2 h
N&T700	1,040°C for 1 h	700°C for 2 h

Mechanical analysis setup

The hardness of the entire sample of 9Cr-1Mo steel was measured using a Vickers microhardness testing machine (INNOVA TEST) with an applied load of 0.30 kgf and 10 s of dwell time, an average of 5 samples was used for each condition. The tensile test specimen (as per ASTM E8/E8M) was prepared [33]. The gauge length and width of the tensile specimens were determined to be 6 mm and 25 mm, respectively. The specimen was made of 9Cr-1Mo steel tubes with an outside diameter of 45 mm and a wall thickness of 3.20 mm. A universal testing machine (Chun Yen) was utilized for static tensile testing at room temperature (STR) and elevated temperature tensile (ETT) testing at a constant cross-head speed of 1 mm min^{-1}. The temperature of the furnace was controlled and maintained within 3 °C for the ETT testing, and the specimen holed the temperature test for 20 min.

Electromagnetic analysis setup

The CEC method may allow evaluation of micro-structural transformation in ferromagnetic material. Any change in structural phase or percentage may affect the electromagnetic characteristics of the materials. In this case, the phase angle and electrical conductivity were measured by the microstructure change. This parameter of the CEC signal is dependent on various factors including microstructure change, local change in the composition and residual stress in the material [17 – 24]. CEC was measured with an OLYMPUS (NORTEC 600) Eddy Current Flow Detector model, which used probe models NEC-2236 / 7L to detect microstructure by phase angle and probe model SPO-887L to detect microstructure by conductivity. The signal phase angles and electroconductivity of the CEC method were measured in the impedance plane, and to statistically improve the results, the measurements were taken from each sample of thermal treatment condition and an average was calculated by obtaining the value for each sample. Finally, the obtained phase angles and electroconductivity were correlated with the grain size, TUTS, and hardness**.**

Results and Discussions

Microstructure characterization

9Cr-1Mo steel (As-received) microstructure is composed of a variety of components such as grain boundary, laths, blocks, packets, sub grains, carbide precipitates, and other precipitates. The grain boundaries are decorated with fine $M_{23}C_6$ in a variety of different morphologies. The fine MX [M: V, Nb, and X: C, N] precipitates were confirmed by the matrix region. The black dotted line in the SEM micrograph, as depicted in Fig. 1(a) and (b), clearly denotes the grain boundaries. In the SEM micrographs shown in Fig. 1(a) and (b) at lower and higher magnifications, the red circles indicate the locations where $M_{23}C_6$ carbide precipitates and fine MX precipitates are found decorated along grain boundaries and in the matrix region. EDS was used to examine the white precipitates that decorate the grain boundaries. The white particles represented in the grain boundary and within the matrix were examined by EDS spectra as shown in Fig. 1(c) and (d). The white particles at the sub grain boundaries were found to contain complementary Cr, Fe, Mo, and Mn compositions, which formed the M23C6 type of carbide precipitation [34], the EDS spectra of the EDS-spot1 as shown in Fig. 1(c). The Cr/Fe ratio of the white particles found at grain boundaries is about 0.297 which suggests that Cr is $M_{23}C_6$

carbide precipitates [34]. In Fig 1(d), the EDS spectra of the EDS-spot2, which exists in the matrix region, demonstrate the formation of fine M23C6 precipitates at the grain boundaries that are lean in Cr, Mo, Mn, and Nb in comparison to $M_{23}C_6$ precipitates at the grain boundaries. The Cr/Fe particle ratio in the matrix was also calculated to be very low at about 0.103. The small particle (MX) that precipitates within the matrix is difficult to identify with the EDS spectra, according to C. Pandey and others [34].

Fig. 2 (a) – (e) presents an optical micrograph of 9Cr-1Mo steel with thermal treatments. The microstructure of the As-received condition using OM that homogeneously dispersed ferrite with C1 + C2 (C1: $M_{23}C_6$, C2: MC) [35 – 36] close to the grain boundary of sized approximately 162.48 μm as shown in Fig. 2(a). The N condition shows the lath martensite structure in form of packets inside of the prior austenite grain boundaries, small upper bainite and the lower bainite as shown in Fig. 2(b). The small particle is observed around the prior austenite grain boundaries. The average grain size was approximately at about 136.83 μm. Fig. 2(c) – (e), shows the OM of samples with N&T conditions. The grain size decreased with increased tempering temperature. The grain size is reduced and measured to be approximately 120.67, 87.81 and 78.30 μm respectively. The small particles are clearly observed form along with the prior austenite grain and the lath boundaries in optical micrographs. The distribution of the small particles is observed in the microstructure of N&T conditions, the dense dispersion was observed with increasing tempering temperature.

The SEM morphology of 9Cr-1Mo steel for different thermal treatment conditions are shown in Fig. 3(a) – (e). For the microstructure of 9Cr-1Mo steel in the As condition, the morphology consists of a ferrite matrix and distribution of carbides precipitates on grain boundaries that are shown in Fig. 3(a). The microstructure in the N condition shows the lath martensitic structure in the form of packets oriented in one direction within prior austenite grain boundaries and coarse precipitates (white particles) distributed on grain boundaries, while inside the matrix region coarser grain are observed, as shown in Fig. 3(b). The thermal treatment condition of 9Cr-1Mo steel results in average particle size and area fraction as shown in Fig. 4. The average particle size and area fraction of carbide precipitates in the N condition were measured to be about 0.735 μm and 17.36%, respectively. In the N&T conditions shown in Fig. 3(c) – (e), the micrographs consist of prior austenite grain boundaries and small boundaries. The average particle size and area

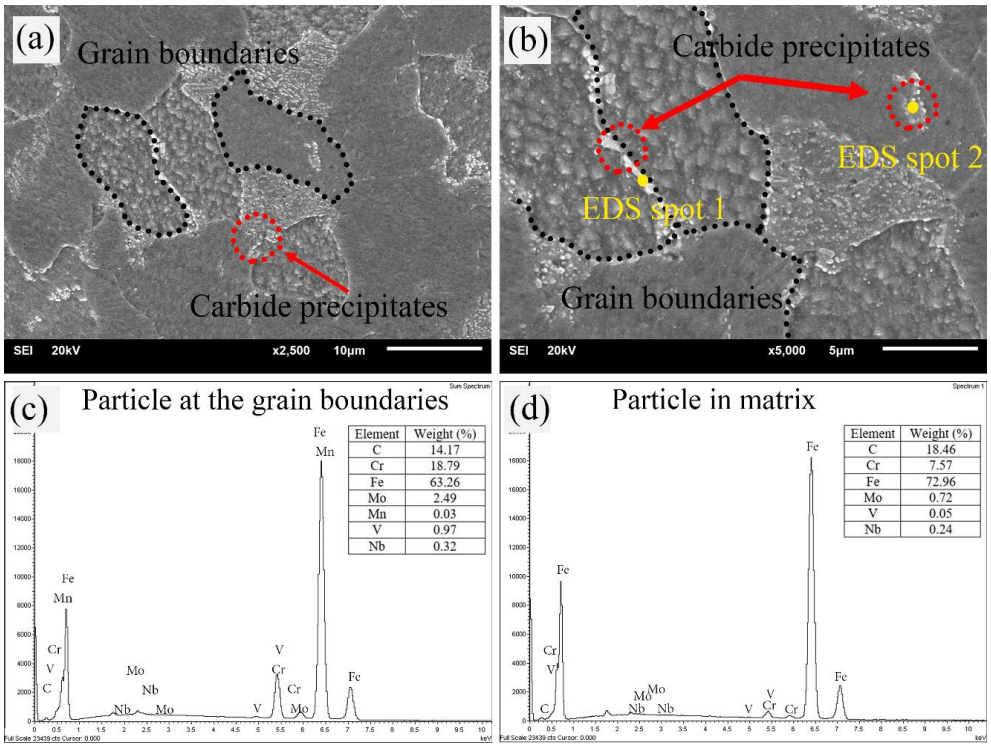

Fig. 1 SEM morphology of 9Cr-1Mo (As-received) at different magnifications indicating carbide precipitates and grain boundaries: (a) at 2500 X, (b) at 5000 X, (c) EDS spectra of white particles present at the grain boundary (EDS-spot1) and (d) EDS spectra of white particles present within the matrix (EDS-spot2).

fraction of carbide precipitates were found to decrease with increased tempering temperature from 600 – 650 °C. For the N&T condition at 700 °C, the average particle size and area fraction of carbide precipitates increased and measured to be approximately 0.13 μm and 15.15%, respectively.

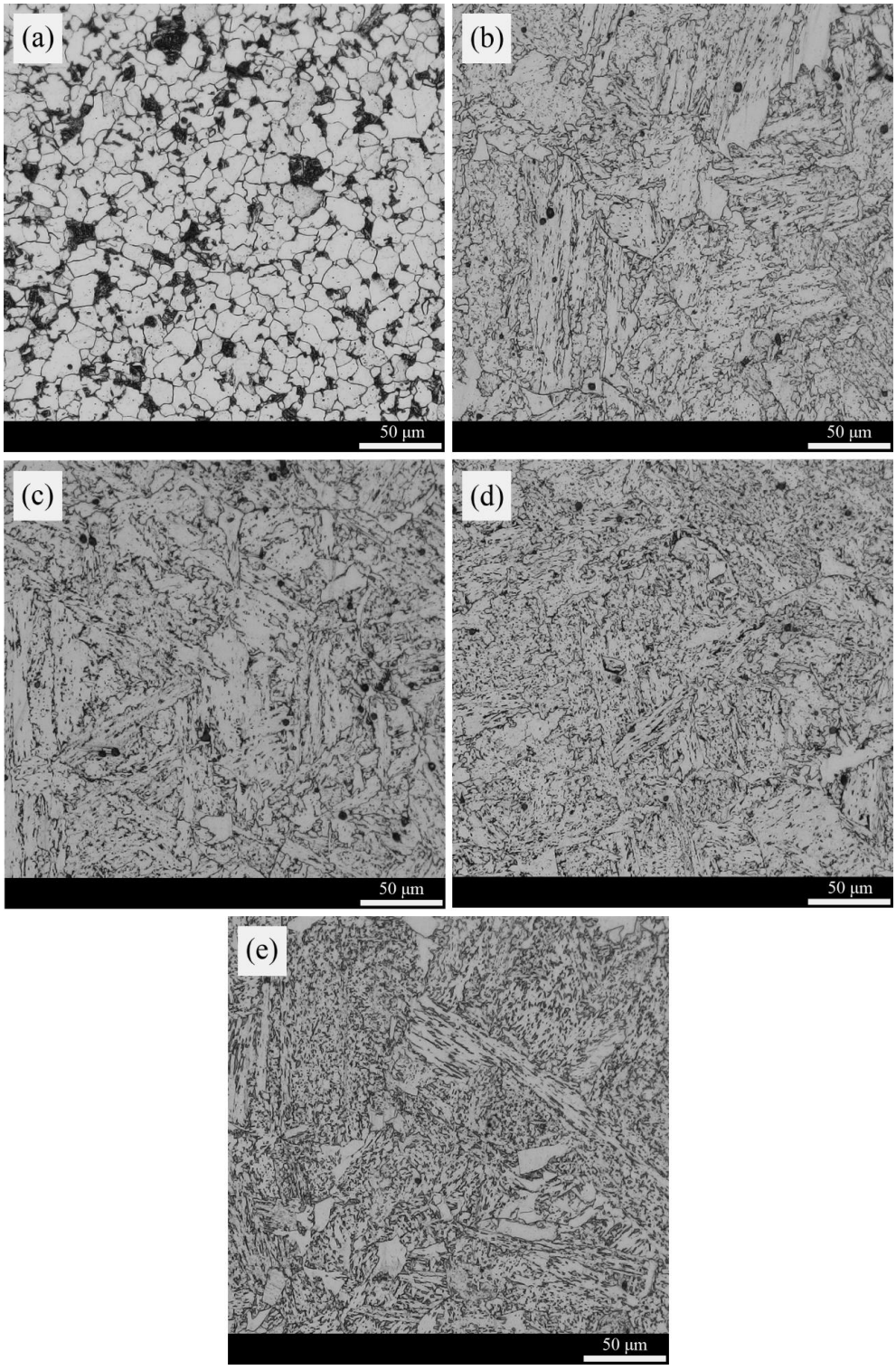

Fig. 2 Optical micrograph of 9Cr-1Mo samples obtained after the different treatments: (a) As, (b) N, (c) N&T600, (d) N&T650, and (e) N&T700.

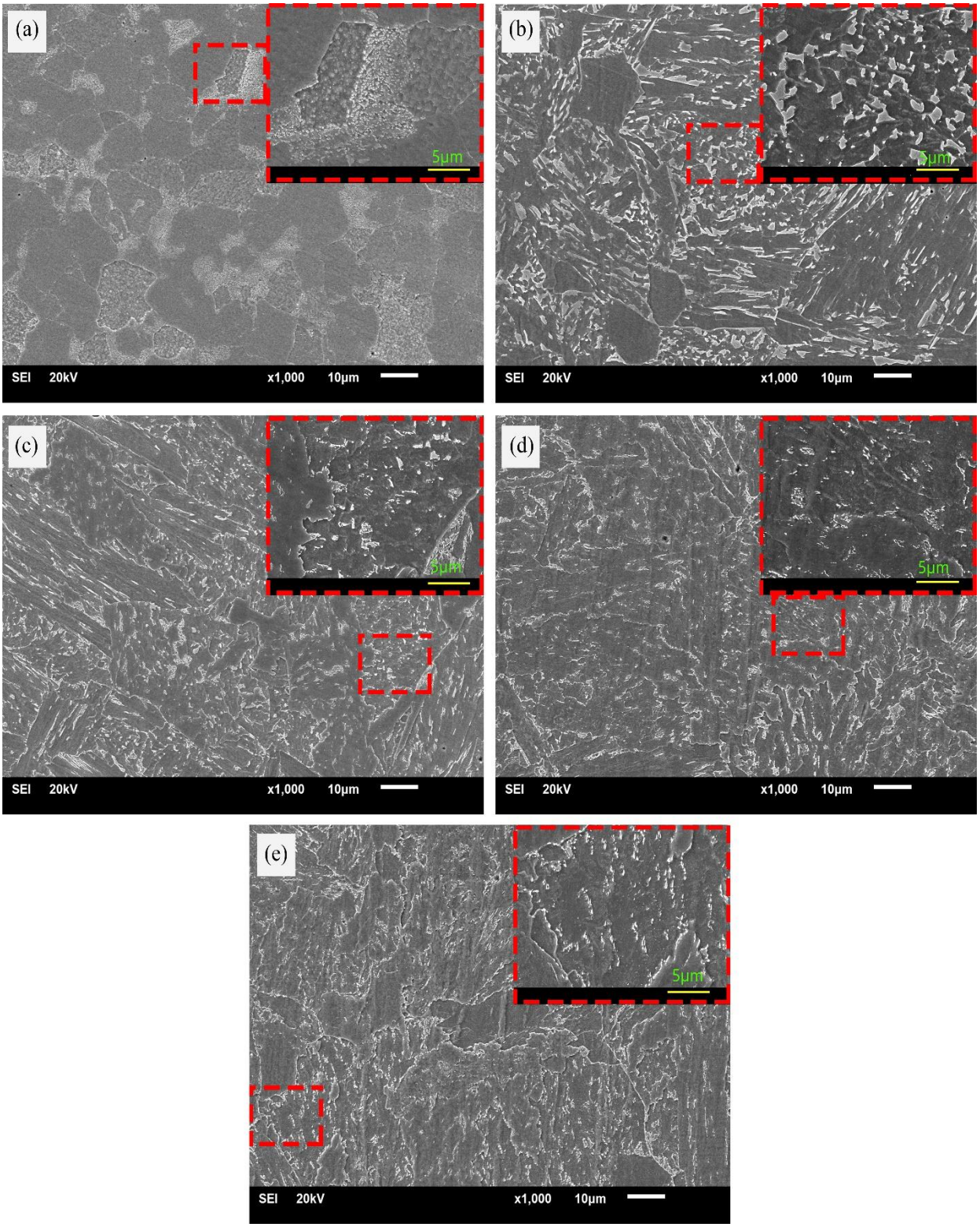

Fig. 3 SEM morphology of 9Cr-1Mo samples obtained after the different treatments: (a) As, (b) N, (c) N&T600, (d) N&T650, and (e) N&T700.

The XRD patterns for 9Cr-1Mo steel as received (As condition) and each thermal treatment condition are shown in Fig. 5. Carbides or carbonitride M_3C, M (C, N), M_2 (C, N), M_7C_3, $M_{23}C_6$ (M stands for metallic solute atoms such as Fe, Cr, Mn, V, Nb, Mo), and other intermetallic precipitates may be observed in 9Cr-1Mo steel. The precipitation sequence for 9Cr-1Mo steel is as follows in equation (1) [37 – 38].

$$\begin{aligned} &M_3C + MC \rightarrow M_3C + MC + M_{23}C_6 \rightarrow \\ &M_{23}C + MC + M_{23}C_6 + M_7C_3 \rightarrow \\ &MC + M_{23}C_6 + M_7C_3 \end{aligned} \quad (1)$$

The XRD pattern indicated in Fig. 4, Mn and Cr-rich $M_{23}C_6$, Fe, Cr, and Mn-rich M_7C_3, Fe - rich M_3C, and Cr-rich M_2X are the phases identified in the As condition of 9Cr-1Mo steel. The XRD pattern remains unchanged after normalization (N condition), but the peak intensity and the number of peaks are reduced. At the lath boundaries, the XRD pattern of the N&T condition resulted in the precipitation of Fe-rich M_3C particles. Further tempering of N&T600 and N&T650 conditions meant that a more stable phase M_7C_3 was observed, which further converted into a stable structure of $M_{23}C_6$. As tempering progressed, the phase M_7C_3 became more stable, eventually converting to the stable structure $M_{23}C_6$. MX carbonitride, $M_{23}C_6$ carbides, M_7C_3 carbides, and M_2X carbonitride precipitates were observed in the final stage of the N&T700 condition. In N&T650 and N&T700, the peaks were seen at the same angles as the As condition, but the $Mn_{23}C_6$ phase had dissolved and no peaks of $Mn_{23}C_6$ could be seen.

The Vicker's microhardness of 9Cr-1Mo steel is shown in Fig. 6. The As condition was measured about 159.84 ± 6.49 HV. The hardness of 9Cr-1Mo steel depends on various terms such as precipitate size, grain size, the density of dislocation in the material, presence of C and N in the solution, and solid solution strengthening [39]. The N condition was found to increase with heat treatment from as-received material. In the N&T conditions, an increase in temperature of tempering after normalizing from 600 – 700 °C resulted in a continuous decrease in hardness of the 9Cr-1Mo steel. However, increased hardness levels of the As and N condition were found to be relatively high compared to samples of N&T conditions in the temperature range from 600 – 700 °C. This may be due to the presence of microstructure transforming the homogeneously dispersed ferrite with C1+C2 (C1: $M_{23}C_6$, C2: MC) in the As condition to have a martensitic structure with the distribution of precipitates and include the higher average particle size and area fraction of precipitates in N condition. In the N&T condition, the variation in hardness with tempering temperature depend on many factors such as the existence of MX type fine precipitates, the size of the grain, the density of the fine precipitates, and the solid solution strengthening caused by the presence of C and N in the solution [40 – 41]. For the N&T condition, an increase in temperature of tempering resulted in a continuous decreased in hardness. Maximum and minimum hardness was measured in the N&T condition about 242.14 and 196.59 HV with tempering temperatures of 600 °C and 700 °C, respectively. Carbides precipitates were seen at the prior austenite grain boundaries, lath boundaries, and in the matrix region as the tempered martensitic structure formed, resulting in a reduction in the solid solution strengthening which reduced the hardness of 9Cr-1Mo steel. The variation in hardness of N&T conditions is fairly well which may be due to the lower average particle size and area fraction of precipitates in the N&T condition.

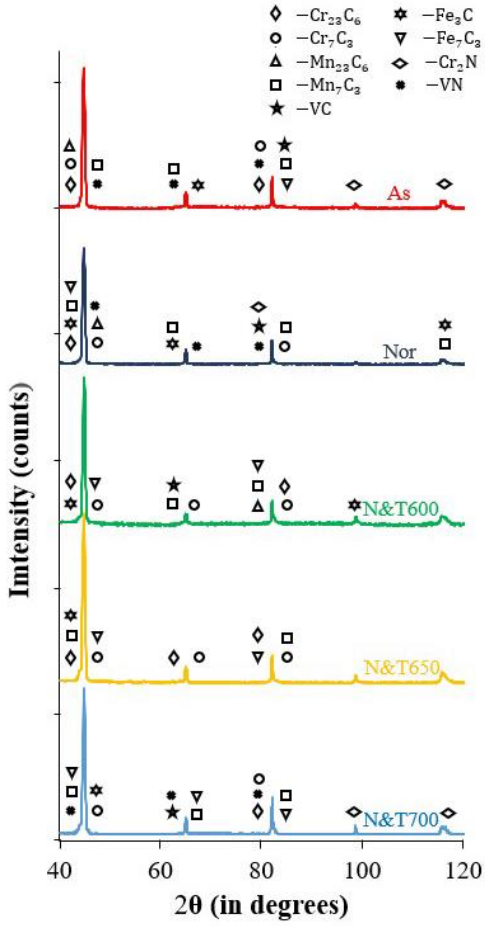

Fig. 5 X-ray diffraction patterns of the 9Cr-1Mo steel: As-received, N condition, N&T600 condition, N&T650 condition, and N&T700 condition.

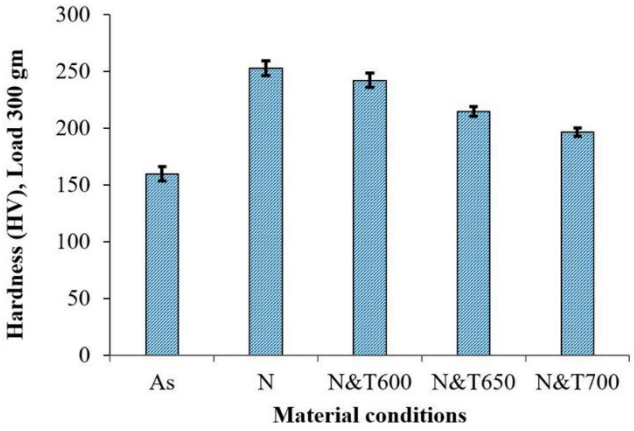

Fig. 6 Hardness of 9Cr-1Mo samples subjected to different material conditions.

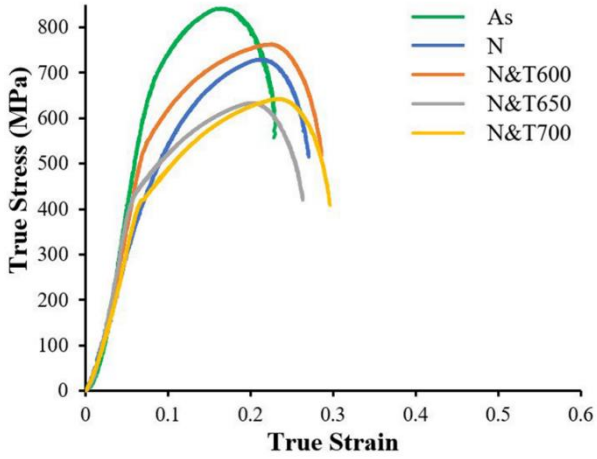

Fig. 7 True stress and true strain of the As-received and thermal treatment conditions of 9Cr-1Mo samples.

Mechanical analysis

The behavior of static tensile testing at room temperature (STR) of 9Cr-1Mo steel with thermal treatment are shown in Fig. 7. The As condition had true yield stress (TYS), true ultimate tensile stress (TUTS), and true strain (TS) were measured about 641.2, 831 MPa, and 0.23, respectively. The trend of TYS and TUTS decreased while TS increased when the thermal treatment condition was used. For the N condition, the effect of TYS and TUTS were about 395.56 and 716.15 MPa, respectively. TYS and TUTS decreased while TS values increased after normalizing because of normalizing reaction, which includes the lath grain boundaries, coarse precipitates on boundaries and in the matrix region coarser grain. For the N&T conditions, TYS, TUTS, and TS decreased in the N&T conditions in the temperature range from 600 – 650 °C, while the N&T700. For tempering temperature from 600 – 650 °C, martensite underwent temperature, and as a result of the tempering reaction, carbides precipitated across prior austenite grain boundaries and lath boundaries. As a result, there was less C and N available in the matrix, which decreased the TYS and TUTS of 9Cr-1Mo steel in the N&T650 condition when compared with the N&T600 condition. This is due to the smaller particle size precipitate and increased precipitate distribution. Centers the matrix and strengthens the solid solution. As a result, the TYS, TUTS, and TS in the N&T700 condition were enhanced, as shown in Fig. 8. The tempering temperature has had a significant impact on the TYS and TUTS. The TYS and TUTS decreased as the tempering temperature increased. Grain size and precipitate size at grain borders have a significant impact on the reduction.

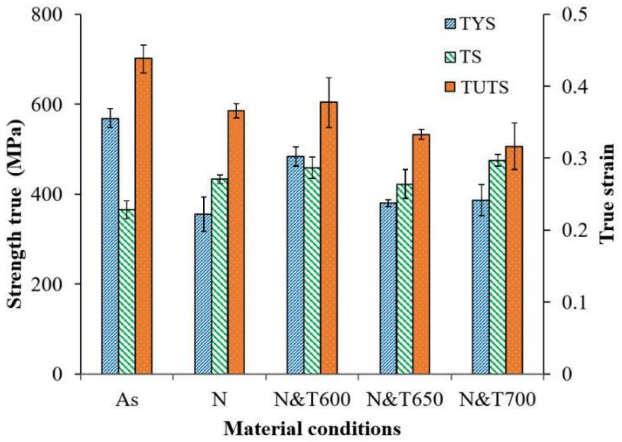

Fig. 8 Static tensile testing of TYS, TUTS, and TS as a function of thermal treatment condition for the 9Cr-1Mo steel at room temperature.

After the tensile test at room temperature, the specimens in each thermal treatment condition were used to study the fracture behavior of specimens using low and high magnification using the SEM technique. The fracture surface of 9Cr-1Mo steel after room temperature static tensile test as shown in Fig. 9. The top right section in each figure represents an overall top view at a magnification of 30X level by using SEM for each thermal treatment condition, as shown in Fig. 9(a) – (g). For the As condition, shown in Fig. 9(a), numerous cracks are noticeable at the fracture surfaces. Large cracks, known as primary cracks, can be seen the radial cracks around the center which are commonly referred to as "splitting" [34, 42] and were also

found at the fracture surface. In the N condition, there was no significant impact on the fracture surface, small secondary cracks were predicted the fracture surface as shown in Fig. 9(b). For the N&T600 condition, a small number of secondary fractures are predicted to have a macroscopic fracture surface as shown in Fig. 9(c). However, after Normalizing (1,040 °C) and tempering at 650 °C, a small secondary fracture was found at the macroscopic fracture surface as shown in Fig. 9(d). When the tempering temperature increased from 650 – 700 °C, very few primary and secondary cracks were seen at the fracture surface as shown in Fig. 9(e).

Fig. 9(a) – (e) provides a detailed view of the fracture surface of 9Cr-1Mo steel after the room temperature static tensile test for each thermal treatment conditions. The appearance of the fracture surface in each thermal treatment condition shows the trans granular with ductile dimples as a result of the incorporation of a microvoids, the fracture of 9Cr-1Mo occurs in ductile material and failed by shear at 45° to an applied load. In every condition, many small particles (inclusions) are observed. When testing by EDS, the inclusions were found to be calcium carbonate which come from the manufacturing process to improve material properties.

The 9Cr-1Mo steel, after undergoing thermal treatment at various conditions and STR testing, was carried out to determine its tensile strength at high temperatures. The test temperatures were 500°C, 550°C, and 600 °C. The behavior of elevated temperature tensile testing (ETT) of 9Cr-1Mo steel with thermal treatment to studies are shown in Fig. 10(a) – (c). The ETT at 500 °C shown in Fig. 10(a) shows that the As condition did not have a very high TUTS compared to the highest TS, while the N condition had the highest TUTS but the least TS. For the N&T condition (600 – 700 °C), the TUTS continuously decreased. While the N&T700 has TS is greater than N&T600 and N&T650. Fig. 10(b) shows the elevated temperature tensile testing at 550°C, which shows that the As condition has the greatest elongation compared to other conditions, however it can be seen that where the N condition is greater than TUTS value. Similarly, with N&T Condition's TUTS which continued to decline. In ETT at 600 °C shown in Fig. 10(c), the specimens in the As condition have the highest TUTS and TS compared to the other specimens which were tested at the same temperature, in which it is evident that the N and N&T specimens have less TUTS when tested at 600 °C.

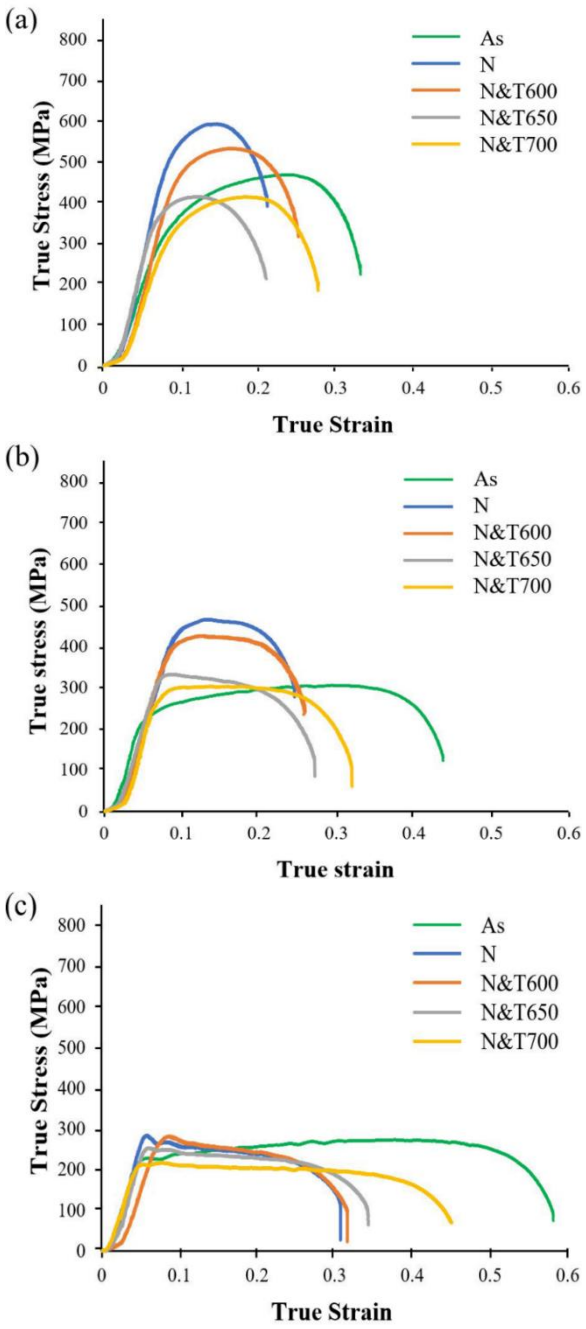

Fig. 10 True stress-strain curve of 9Cr-1M0 steel when the tensile test was conducted at (a) 500 °C, (b) 550 °C, and (c) 600 °C.

Electromagnetic analysis

Prior to using electromagnetic analysis with eddy current techniques, the 9Cr-1Mo steel must be evaluated to find an appropriate frequency to recognize and distinguish the resulting eddy current signal by increasing the frequency

in the range of 50 – 150 kHz. Table 3 shows the change in the phase angle signal of the eddy current signal.

Table 3 The signal phase angle changes in each material condition

Material condition	Frequency (kHz)		
	50	100	150
As	60.12	49.22	15.21
N	41.95	44.10	31.65
N&T600	48.10	47.12	31.04
N&T650	39.07	48.19	31.57
N&T700	40.63	50.72	30.14

In this situation, the frequency of 100 kHz was selected since it indicates the maximum association between the microstructure of each thermal treatment condition. The structure of 9Cr-1Mo steel when it transformed the microstructure was verified by the CEC. The CEC signal was compared between the two parameters using a phase angle change and conductivity versus grain size of 9Cr-1Mo in each thermal treatment condition at a frequency of 100 kHz, as shown in Fig. 11. The results show that using the CEC test at the same frequency to detect the grain size. The conductivity change in the material was more accurate than testing by measuring with phase angle. The signal of conductivity and phase angle increases with the increasing the grain size of 9Cr-1Mo in each thermal treatment condition. The correlation coefficient is 0.9224 and 0.847, respectively. Since the signals phase angle, conductivity, and TUTS are associated with changes that occur in the microstructure of 9Cr-1Mo steel in each thermal treatment condition specimen during increases the thermal treatment.

Fig. 13 shows the change in phase angle and conductivity of the CEC signal as a function of hardness properties in each thermal treatment affected in terms of N and N&T conditions. The signal of phase angle and conductivity decreases with increasing microhardness. Signal phase angle and conductivity have a correlation value of 0.8826 and 0.8885, respectively.

The relationships between signal phase angle, conductivity, and TUTS are shown in Fig. 12. When the material is subjected to increasing thermal treatment (N and N&T), the area fraction of carbide in 9Cr-1Mo steel increases while the dispersed carbide size decreases, resulting in enhanced TUTS. The signal phase angle and the TUTS of the materials were found to have a high signal fluctuation that could not be interpreted in the test results, although the signal conductivity in each condition grows as the TUTS of the material conditions increases. The correlation coefficient of signal phase angle and conductivity are 0.4066 and 0.9459, respectively.

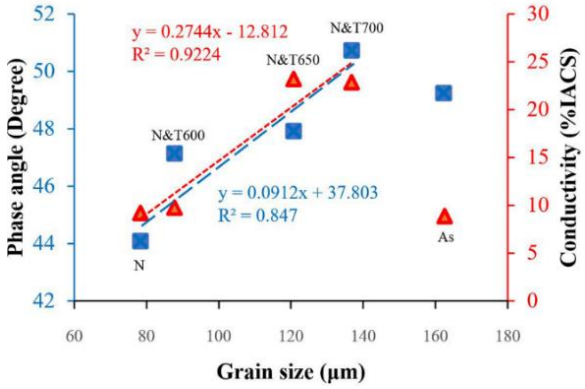

Fig. 11 Signal phase angle and conductivity versus grain size.

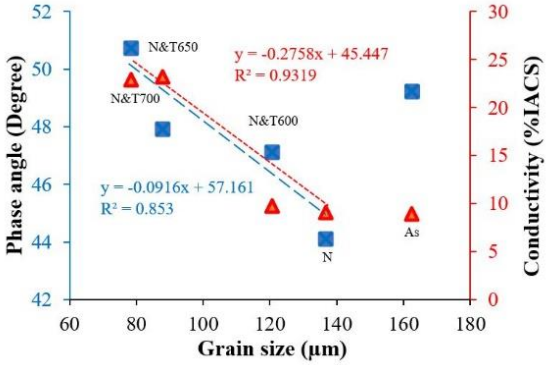

Fig. 12 The signal phase angle, conductivity, and TUTS of 9Cr-1Mo steel.

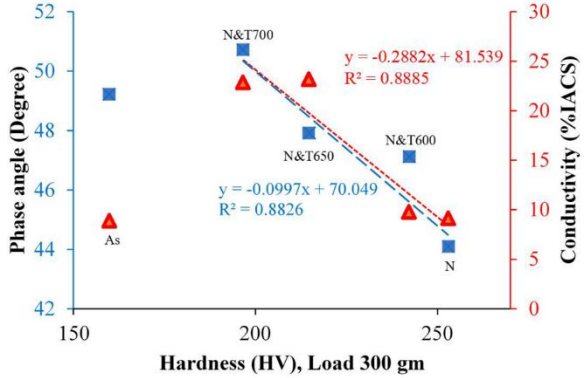

Fig. 13 The signal phase angle and conductivity versus microhardness with a load of 300 g.

Conclusion

This study investigated the effects of different thermal treatments on the microstructures and hardness of 9Cr-1Mo steel. The microstructures of the as-received steel were changed from the ferrite with C1+C2 (C1: $M_{23}C_6$, C2: MC) structures to the lath martensite, prior austenite grain boundaries, small upper bainite and lower bainite after being tempered.

When increasing the tempering temperature, the size of carbide precipitates and area fraction of precipitates decreased dramatically. However, the area fraction of precipitates began to increase when a tempering temperature of 700°C was employed. Hence, the tempering temperature had to be lower than 700°C keep the area fraction of carbide precipitate small.

In the XRD pattern, carbides precipitate of $M_{23}C_6$ and M_7C_3 structures were also observed in each state of thermal treatment condition. With increasing tempering time, the M_2X phase is gradually replaced by more thermally stable $M_{23}C_6$ particles. In each state of heat treatment, the M_3C phase was found, but the number of counts in XRD analysis was found to be reduced after the N&T650 condition.

In addition, the hardness and stresses of 9Cr-1Mo steel were found to decrease with increases in tempering temperature. The eddy current method was used in the investigation to characterize the metal structures. The use of CEC with a proper conductivity was able to more accurately detect the microstructural changes of 9Cr-1Mo samples examined in this study than using the phase angle approach. Thus, the proposed NDT technique could replace the replica method which is detrimental to the sample surface during the test.

Acknowledgement

The authors are thankful for the financial and technical support from the Department of Production Engineering, Materials and Nondestructive Testing Laboratory (MNDT) and the Innovative environmental management and smart construction materials Laboratory (IEM) at KMUTT Ratchaburi learning park.

References

[1] R. Viswanathan, W. Bakker, Materials for ultra-supercritical coal power plants boiler materials: part 1, J. Mater. Eng. Perform. 10 (2001) 81 – 95.

[2] C. Coussment, A. Dhooge, M. de Witte, R. Dobbelaere, E. van der Donckt, High temperature properties of improved 9% Cr steel weldments, Int. J. Press. Vessel. Pip. 45(2) (1991) 163 – 178.

[3] H.B. Sata, G. Amarendra, R. Rajaraman, C.S. Sundar, Microstructural characterization of ferritic/martensitic steel by positron annihilation spectroscopy, J Phys Conf Ser. 443 (2013) 1 – 6.

[4] S. Mannan, S.C. Chetal, B. Raj, S. Bhoje, Selection of Material for Prototype Fast Breeder Reactor, Trans. Indian Inst. Met. 56 (2003) 155 – 178.

[5] F. Masuyama, History of Power Plants and Progress in Heat Resistant Steels, ISIJ Int. 10 (6) (2001) 612 – 625.

[6] M.E. Abd El-Azim, A.M. Nasreldin, G. Zies, A. Klenk, Microstructural instability of a welded joint in P91 steel during creep at 600 °C, Mater. Sci. Technol. 21(7) (2005) 779 – 790.

[7] A. Mitra, J.N. Mohapatra, J. Swaminathan, M. Ghosh, A.K. Panda and R.N. Ghosh, Magnetic evaluation of creep in modified 9Cr-1Mo steel, Scr. Mater. 57(9) (2007) 813 – 816.

[8] F. Sket, K. Dzieciol, A. Borbely, A.R. Kaysser-pyzalla, K. Maile, R. Scheck, Microtomo-graphic investigation of damage in E911 steel after long term creep, Int. J. Mater. Res. 528(1) (2010) 103 – 111.

[9] C. Pandey, M.M. Mahapatra, P. Kumar, N. Saini, Effect of normalization and tempering on microstructure and mechanical properties of V - groove and narrow - groove P91 pipe weldments, Mater. Sci. Eng. A. 685 (2017) 39 – 49.

[10] P. Mohyla, Z. Kubon, R. Cep, I. Samardzic, Evaluation of Creep Properties of Steel P92 and Its Welded Joint, Metalurgija. 53(2) (2014) 175 – 178.

[11] H.K.D.H. Bhadeshia, A. Strang, D.J. Gooch, Ferritic power plant steels: remanent life assessment and approach to equilibrium, Int. Mater. Rev.43 (2013) 45 – 69.

[12] K.S. Chandravathi, K. Laha, K. Bhanu Sankara Rao, S. Mannan, Microstructure and tensile properties of modified 9Cr–1Mo steel (grade 91), Mater. Sci. Technol. 17(5) (2001) 559 – 565.

[13] Y. Jaluria, Chapter One - Heat and Mass Transfer in Materials Processing and Manufacturing, Adv. Heat Transf. 48 (2016) 1 – 94.

[14] R.J. Seher, G. N. Maniar, Analytical-preshadowed extraction replica technique. Metallography, Metallogr. 5(5) (1972) 409 – 414.

[15] S. Jana, Non-destructive in-situ replication metallography, J Mater Process Technol. 49(1-2) (1993) 85 – 114.

[16] K. Mariappan, V. Shankar, R. Sandhy, M.D. Mathew, A.K. Bhaduri, Influence of Prior Fatigue Damage on Tensile Properties of 316L(N) Stainless Steel and Modified 9Cr-1Mo Steel, Metall Mater Trans A Phys Metall Mater Sci. 46 (2014) 989 – 1003.

[17] D.J. Hagemair, Fundamentals of eddy current testing, Amer Society for Nondestructive, (1990) 1 - 92.

[18] C. S. Kim, Nondestructive Evaluation by Reversible Magnetic Permeability of the Residual Life of Ferritic 9Cr Steel Subjected to Creep-Fatigue Damage, Mater Trans. 59 (2017) 316 – 319.

[19] A. Sahebalam, M. Kashefi, S. Kahrobaee, Comparative study of eddy current and Barkhausen noise methods in microstructural assessment of heat treated steel parts, Nondestruct. Test. Evaluation. 29 (2014) 208 – 218.

[20] M. Oka, Y. Tsuchida, T. Yakushiji, M.Enokizono, Fatigue Evaluation for a Ferritic Stainless Steel (SUS430) by the Eddy Current Method Using the Pancake-Type Coil. IEEE Trans. Magn. 46(2) (2010) 540 – 543.

[21] D. Kukla, A. Bałkowiec, P. Grzywna, Evaluation of Microstructural Changes of S235 Steel after Rolling on the Basis of Microscopic Observations and Eddy Current Non-Destructive Method, Adv. Mater. Sci., 14 (2014) 40 – 48.

[22] M. Kashefi, S. Kahrobaee, M.H. Nateq, On the Relationship of Magnetic Response to Microstructure in Cast Iron and Steel Parts, J. Mater. Eng. Perform. 21 (2012) 1520 – 1525.

[23] J. Liu, J. Wilson, M. Strangwood,C. L. Davis, Magnetic characterization of microstructural feature distribution in P9 and T22 steels by major and minor BH loop measurements, J. Magn. Magn. Mater. 401 (2016) 579 – 592.

[24] J. Liu, M. Strangwood, C. L. Davis, A.J. Peyton, Magnetic Evaluation of Microstructure Changes in 9Cr-1Mo and 2.25Cr-1Mo Steels Using Electromagnetic Sensors, Metall Mater Trans A Phys Metall Mater Sci. 44(13) (2013) 5897 – 5909.

[25] F. Abe, 9Cr-1Mo steel, in K. Yagi, G. Merckling, T.-U. Kern, H. Irie, H. Warlimont (Eds.), Landolt-Börnstein - Group VIII Advanced Materials and Technologies 2B (Creep Properties of Heat Resistant Steels and Superalloys), 2004, Vol 2B, pp, 118 – 125.

[26] J. Arndt, K. Haarmann, G. Kottmann, J. C. Vaillant, W. Bendick, F. Deshayes, Thermal Power Plants, Janeza Trdine 9, Rijeka, Croatia, 51000.

[27] ASTM, I A213/A213M − 18: Standard Specification for Seamless Ferritic and Austenitic Alloy-Steel Boiler, Superheater, and Heat-Exchanger Tubes1, West Conshohocken, PA, USA: ASTM International, 2018.

[28] M. Song, C. Sun, Y. Chen, Z. Shang, J. Li, Z. Fan, K. T. Hartwig and X. Zhang, Grain refinement mechanisms and strength-hardness correlation of ultra-fine grained grade 91 steel processed by equal channel angular extrusion, Int. J. Press. Vessel. Pip. 172 (2019) 212 – 219.

[29] N. Saini, C. Pandey, M.M. Mahapatra, Characterization and evaluation of mechanical properties of CSEF P92 steel for varying normalizing temperature, Mater. Sci. Eng. A. 688 (2017) 250 – 261.

[30] D.R. Barbadikar, G.S. Deshmukh, L. Maddi, K. Laha, P. Parameswaran, A.R. Ballal, D.R. Peshwe, R.K. Paretkar, M. Nandagopal, M.D. Mathew, Effect of normalizing and tempering temperatures on microstructure and mechanical properties of P92 steel, Int. J. Press. Vessel. Pip. Vol. 132 (2015) 97 – 105.

[31] N. Saini, C. Pandey, M.M. Mahapatra, R.S. Mulik, On study of effect of varying tempering temperature and notch geometry on fracture surface morphology of P911 (9Cr-1Mo-1W-V-Nb) steel, Eng Fail Anal. 85 (2018) 104 – 115.

[32] N. Saini, C. Pandey, M.M. Mahapatra, R. S. Mulik, Evolution of nano-size precipitates during tempering of 9Cr-1Mo-1W-V-Nb steel and their influence on mechanical properties, Mater. Sci. Eng. A 711 (2018) 37 – 43.

[33] ASTM, I. ASTM E8/E8M-16a: standard test methods for tension testing of metallic materials. West Conshohocken, PA, USA: ASTM International, 2016.

[34] C. Pandey, A. Giri, M.M. Mahapattra, Evolution of phases in P91 steel in various heat treatment conditions and their effect on microstructure stability and mechanical properties, Mater. Sci. Eng. A. 664 (2016) 58 – 74.

[35] E. Ayala, M.A. Roman., Roman, J. Vega, X. Gomez, T. Genez-Acebo, J. Echberria, Delta ferrite formation in 9–12% chromium steel weldments, In Advanced heat resistant steels for power generation (San Sebastian, 27-29 April 1998, preprints) 1998.

[36] X. Chai, J.C. Bundy, M.A. Amata, C. Zhang, F. Zhang, S. Chen, S. S. Babu, S.Kou, Creep Rupture Performance of Welds of P91 Pipe Steel, Weld J. 94(5) (2015) 145 – 157.

[37] N. Fujita, H.K.D.H. Bhadeshia, Modelling simultaneous alloy carbide sequence in power plant steels, ISIJ Int. 42(7) (2002) 760 – 769.

[38] A. Baltušnikas, R. Levinskas, I. Lukoštūtė, Kinetics of Carbide Formation During Ageing of Pearlitic 12X 1МФ steel, J. Mater. Sci. 13(4) (2007) 286 – 292.

[39] C. Pandey, A. Giri, M.M. Mahapatara, Effect of normalizing temperature on microstructural stability and mechanical properties of creep strength enhanced ferritic P91 steel, Mater. Sci. Eng. A. 657(7) (2016) 173 – 184.

[40] C. Pandey, M.M. Mahapatara, Effect of long-term ageing on the microstructure and mechanical properties of creep strength enhanced ferritic P91 steel, Trans. Indian Inst. Met. 69 (2016) 1657 – 1673.

[41] C. Pandey, M.M. Mahapatara, Effect of soaking temperature and time on microstructure and mechanical properties of P91steel, in: Proceedings of the 23 rd International Conference on Processing and Fabrication of Advanced Materials, IIT Roorkee, India, 2014.

[42] C. Hurtado, C.A. Danon, M. Luppo, P. Bruzzoni, Evolution of minor phase sigma 9Pct Cr steel: effect of tempering temperature and relation with hydrogen trapping, Metall Mater Trans. 46(9) (2015) 3972 – 3988.